

# Simulating Acoustic Orientation Trapping for Stable Levitation

Petteri Helander<sup>1</sup>, Tuomas Puranen<sup>1</sup>, Antti Meriläinen<sup>1</sup>, Göran Maconi<sup>1</sup>, Antti Penttilä<sup>1</sup>,  
Maria Gritsevich<sup>1,2,3</sup>, Ivan Kassamakov<sup>1</sup>, Ari Salmi<sup>1</sup>, Karri Muinonen<sup>1,3</sup>, Edward Hægström<sup>1</sup>

<sup>1</sup>Department of Physics, University of Helsinki, Helsinki, Finland

<sup>2</sup>Institute of Physics and Technology, Ural Federal University, Ekaterinburg, Russia

<sup>3</sup>Finnish Geospatial Research Institute FGI, Masala, Finland

Email: petteri.helander@helsinki.fi, ari.salmi@helsinki.fi

**Abstract**—Acoustic levitation permits non-contact handling of mm-scale samples. To improve its applicability, we did a simulation study to optimize orientation control of a sample residing in a phased array levitator. The acoustic forces and torques on asymmetric samples in asymmetric traps were determined by solving the acoustic scattering problem with the boundary element method. The angular stiffness of the trap was mapped as a function of the field shape. This allowed us to choose the optimal incidence field for different shaped samples. A mathematical model was created that predicts the results with good agreement.

**Index Terms**—acoustic levitation, acoustic radiation force, boundary element method

## I. INTRODUCTION

Acoustic levitation permits non-contact manipulation of mm-scale samples [1]. This is valuable for chemistry and life sciences where the samples are macroscopic, and contamination can be unacceptable [2]. Unlike other levitation techniques, acoustic levitation is compatible with any solid or liquid material. In addition, acoustic levitation is affordable and scalable, as the levitation devices have migrated from single transmitter-reflector systems to large phased array transducer (PAT) levitators [3].

Despite its advantages and progress on PATs, acoustic levitation has not been widely adapted. One shortcoming is the lack of reliability. A small disruption in the system can introduce large sample oscillations. Another issue is lack of rotation control. Until now only limited orientation locking in one plane has been demonstrated [4]. Improved rotation control would make levitation more robust and allow combining it with existing advanced characterization methods [5, 6], such as X-ray tomography.

We recently developed an acoustic levitation method capable of full 3-axis orientation control of asymmetric samples [7]. This was achieved with a spatially asymmetric vortex trap created with PAT, whose phases and amplitudes were set according to our method. Although we demonstrated rotation control, driving the method to its limits requires one to understand the details of the acoustic radiation force acting on the sample. In this current work we developed a simulation model to calculate the acoustic torques for a sample with arbitrary shape. This allows us to tune the acoustic trap shape to achieve maximum sample stability.

## II. ACOUSTIC RADIATION TORQUE

Acoustic radiation force originates from the small amount of momentum carried by acoustic waves. The phenomenon is prominent in a standing wave field for samples smaller than the half wavelength. The generated forces are typically described using Gor'kov potential, a simplified mathematical model [8]. This approach, however, is only valid for small rigid spheres and does not consider torques. For real particles, the acoustic scattering problem must be solved numerically to obtain the pressure field  $P$  and acoustic velocity field  $V$ . To do this, frequency domain boundary element method (BEM) simulation was carried out using COMSOL Multiphysics® (version 5.3) Pressure Acoustics interface. BEM allows one to omit modeling the surrounding air domain and thus reduces

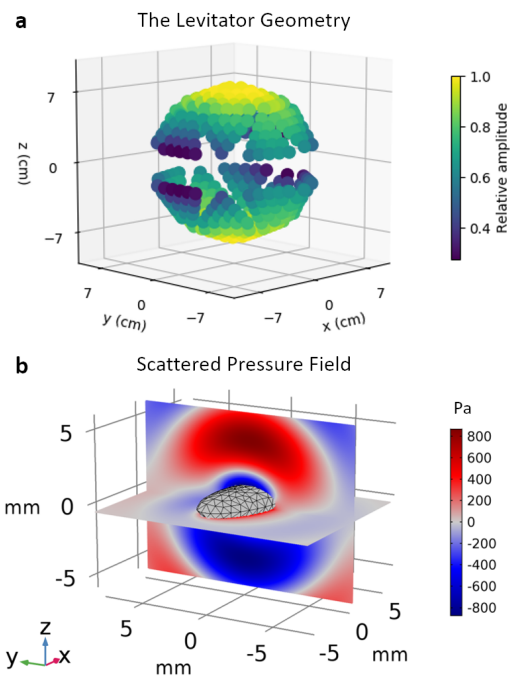


Fig. 1. **a)** Phased array levitator geometry and transducer amplitudes. Asymmetric amplitudes enable the orientation control. **b)** Scattered pressure field around the levitated particle, a slightly orientated ellipsoid. A vortex-like pattern is observed.

computation time. With finite element method (FEM) extra care is needed to eliminate unwanted reflections from model boundaries, whereas in BEM this happens inherently.

The model was constructed based an existing device with 450 acoustic transducers (frequency band  $(40 \pm 1)$  kHz). The transducers were arranged first in modules (15 transducers in a module, 30 modules) and then in two hemispheres, Fig 1a. Each transducer was modelled as a point source (*background pressure field*) with individually set phase and amplitude. All simulations were run with fixed frequency  $\omega = 2\pi \cdot 40$  kHz as this was the one used experimentally, resulting in wavelength  $\lambda \approx 8.6$  mm. Due to the large number of transducers, the creation of the model was automated with LiveLink™ for MATLAB®. The created field shape was described with one parameter, the pressure gradient ratio along the principal axis of the trap,  $\alpha = \partial_y p_{\max} / \partial_z p_{\max}$ . The pressure amplitude of the field was 3 kPa with the value of  $z$ -gradient being fixed.

The levitated particle (Fig 1b) was introduced as an empty void and thus its walls are acoustically hard (*sound hard boundary*,  $\mathbf{V} \cdot \mathbf{n} = 0$ ). This was done to simplify the interpretation of the results. Ellipsoids with varying size and aspect ratio were used as test samples. The sample was placed in the pressure node at the center of the levitator. To apply an acoustic torque, the sample was displaced from its equilibrium orientation by 15 degrees. This was repeated for rotation around each axis. The pressure and velocity fields were then solved.

The acoustic radiation force is a second order effect. The acoustic part of the field,  $P_1$ , creates large forces, but they are averaged out over one full cycle in time. The particle dynamics are much slower, and the particle only feels the time averaged second order perturbation  $P_2$ . The effective force and torque can be expressed using first order harmonic fields [9]:

$$\mathbf{F} = \oint_{A_e} dA \left\langle \underbrace{-\rho(\mathbf{V} \cdot \hat{\mathbf{n}})\mathbf{V} - \frac{1}{2\rho c^2} P^2 \hat{\mathbf{n}} + \frac{1}{2}\rho V^2 \hat{\mathbf{n}}}_{d\mathbf{F}} \right\rangle, \quad (1)$$

$$\boldsymbol{\tau} = \oint_{A_e} \mathbf{r} \times d\mathbf{F}. \quad (2)$$

Here  $\rho = 1.34 \text{ kg/m}^3$  is the density of air,  $c = 343 \text{ m/s}$  is the speed of sound in air,  $\hat{\mathbf{n}}$  is the normal vector pointing out and  $\langle \rangle$  stands for time averaging. The integration can be done across any surface  $A_e$  that encloses the levitated particle, as the liquid is considered inviscous and thus angular momentum is conserved [10]. The expression  $d\mathbf{F}$  was evaluated on the surface of the particle to gain insight about the distribution of forces. The actual integration was done on an enclosing spherical surface  $A_e$  ( $r = 7 \text{ mm}$ ) to ensure numerical validity. The small surface was chosen to minimize the meshing requirement since the radiation pattern becomes complex further away.

To increase numerical accuracy, Eq. 2 was simplified as

$$\boldsymbol{\tau} = \oint_{A_e} dA \mathbf{r} \times \langle -\rho(\mathbf{V} \cdot \mathbf{n})\mathbf{V} \rangle, \quad (3)$$

$$\tau_i = -\frac{\rho}{2} \oint_{A_e} dA \epsilon_{ijk} r_j n_m \text{Re}\{v_m^{\text{sc}} v_k^{\text{in}*} + v_m^{\text{in}} v_k^{\text{sc}*} + v_m^{\text{sc}} v_k^{\text{sc}*}\}. \quad (4)$$

We divided the harmonic field  $\mathbf{V}$  into an incident field  $\mathbf{V}^{\text{in}}$  and scattered field  $\mathbf{V}^{\text{sc}}$ , and  $\epsilon_{ijk}$  is the Levi-Civita symbol for the Einstein sum notation. We omit the term with incidence field squared ( $v_m^{\text{sc}} v_k^{\text{sc}*}$ ) as the incident field can not carry momentum into the region on average. In addition, we made the expression compatible with the frequency domain BEM solver that provides the complex valued velocity field  $\mathbf{v}$  such that  $\mathbf{V}^{\text{in}} = \text{Re}\{\mathbf{v}^{\text{in}} e^{i\omega t}\}$  and  $\mathbf{V}^{\text{sc}} = \text{Re}\{\mathbf{v}^{\text{sc}} e^{i\omega t}\}$ . The numerical integration was done within the simulation software. The integration was repeated on another enclosing surface to ensure the validity of the result via conservation of angular momentum. A convergence study for mesh size was done.

### III. RESULTS AND DISCUSSION

The Gor'kov potential for a sphere with volume  $V_p$ ,

$$U_{\text{Gor'kov}} = V_p \left( \frac{1}{2\rho c^2} \langle P^2 \rangle - \frac{3}{4}\rho \langle V^2 \rangle \right), \quad (5)$$

helps one understand the orientation control method even though it cannot be used to calculate the torques. In Fig. 2 the potential is presented for three values of the pressure gradient ratio  $\alpha$  with  $V_p = \frac{4}{3}\pi(1 \text{ mm}/2)^3$ . The regions with high value of potential repel the particle whereas the low valued potential well attracts it. For  $\alpha = 1$  the field is symmetric in the  $yz$ -plane and thus cannot lock rotation around  $x$ -axis. For  $\alpha = 0$  there is symmetry in the  $xy$ -plane and therefore no torques

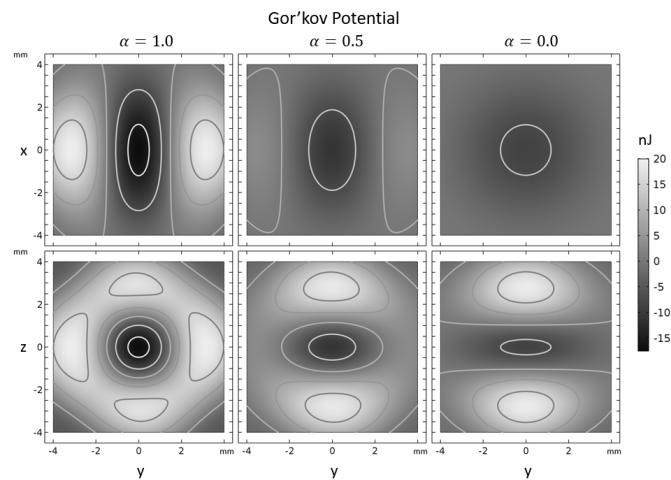


Fig. 2. Cross sections of Gor'kov potential of the trap created with our phase calculation method. Top row is top view, bottom row is front view. The contours are drawn with 7.5 nJ interval. Changing the  $\alpha$  parameter affects the trap aspect ratio. For  $\alpha = 1$  it introduces  $yz$ -symmetry, whereas with  $\alpha = 0$   $xy$ -symmetry is created.

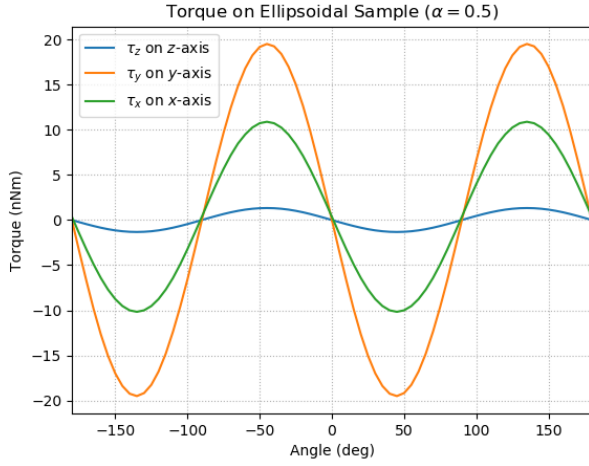


Fig. 3. The acoustic torque on an ellipsoid with dimension  $r_x = 1.5$  mm,  $r_y = 0.8$  mm,  $r_z = 0.4$  mm. The field asymmetry was set  $\alpha = 0.5$ . The stable equilibrium orientations lie at zero degrees and 180 degrees. The orientations at  $\pm 90$  degrees are unstable equilibria.

around the  $z$ -axis. The values between, e.g. the center column, create an ellipsoidal field which should be capable of locking the orientation of an ellipsoid sample.

The torque projected on an ellipsoid in the center column trap of Fig. 2 is shown in Fig. 3 as a function of deflection angle from the equilibrium orientation. Each curve has its maximum at 45 degrees and an unstable minimum at 90 degrees. The magnitude of the torques spans one decade with

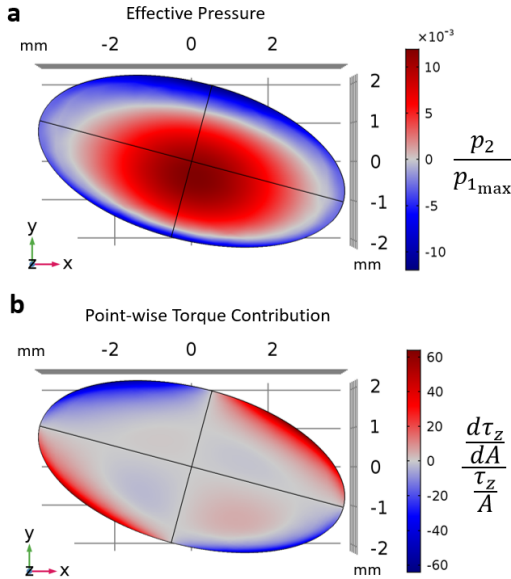


Fig. 4. **a)** The second order pressure that causes the forces after time averaging, expressed as ratio to maximum acoustic pressure (3 kPa). The pressure node is located in the origin and the vortex incidence field lies in  $yz$ -plane. Field asymmetry  $\alpha = 0.6$  **b)** The  $z$ -component of the acoustic torque along the surface, normalized to total torque (23 nNm).

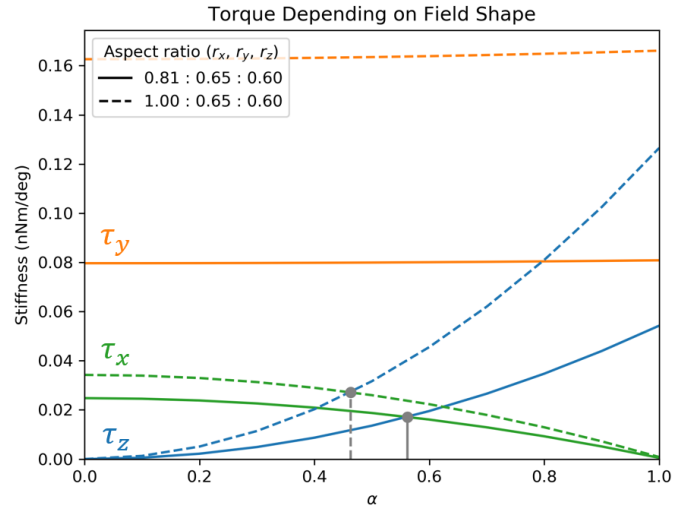


Fig. 5. Trap stiffness as a function of  $\alpha$  for two ellipsoids with different aspect ratio. The optimal stiffness is the crossing point of  $\tau_z$  and  $\tau_x$ .

$\tau_z$  being the smallest,  $\tau_y$  the largest and  $\tau_x$  in between. However, from the symmetry properties of the field, it is expected that changing  $\alpha$  will flip the order of  $\tau_z$ , and  $\tau_x$ .

The slope of the curve at zero is the rotational stiffness  $k$  of the trap. The linearity of the force close to the proximity of the equilibrium causes the particle to behave as a harmonic oscillator with resonance frequency  $2\pi f_i = \sqrt{\frac{k_i}{I_i}}$  around the  $i$ -axis. Here  $I_i$  is the moment of inertia. Table 1 shows the resonances in a case where the density of the sample in Fig. 3 equals that of water.

TABLE I  
SAMPLE VIBRATION PROPERTIES

Axis	Stiffness (pNm/deg)	Resonant frequency (Hz)
$x$	370	40
$y$	680	30
$z$	50	8

Fig. 4 shows acoustic forces and torques along the surface of the levitated particle. This illustrates the origin of the torque more truthfully than the supposed alignment in the Gor'kov potential. In Fig. 4a the time-averaged second order pressure  $p_2$  shows that the particle is pushed towards origo both from top and bottom and that it is sucked from all sides. The non-linearity,  $\frac{p_2}{p_1}$ , is 1% at maximum. The ellipsoid was deflected 15 degrees around the  $z$ -axis and the corresponding torque was plotted point-wise in Fig. 4b. The integration over the surface mostly cancels out, but a small restoring torque remains.

The dependency of the stiffness of the trap on the field shape is shown in Fig. 5. The  $\tau_y$  is largely unaffected, unlike  $\tau_x$  and  $\tau_z$ . As expected, the two stiffnesses cross for a certain  $\alpha$ . By choosing the value of  $\alpha$  in crossing point, one maximizes the trap stiffness. This value of  $\alpha$  we define as the optimal one,  $\alpha_1$ , which is a function of the ellipsoid shape.

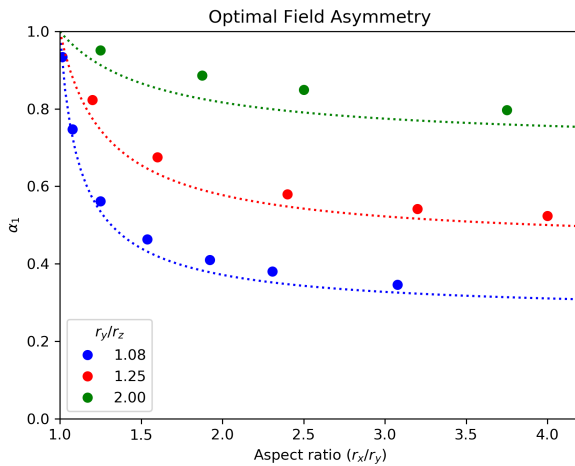


Fig. 6. The optimal field shape as function of the sample shape. The dashed curves are the theoretical predictions.

In Fig. 6 the optimal field shape  $\alpha_1$  is plotted for different ellipsoids. The more disc like the particle (small  $r_x/r_y$  and large  $r_y/r_z$ ) the larger  $\alpha$  should be. Vice versa, for a stick-like particle a small  $\alpha$  is preferred. If free rotation around the symmetry axis of the disc or stick is allowed, the field asymmetry can be set the other way around to lock the other two rotation angles better. A mathematical model is plotted together with the simulation results. The model is constructed with the assumption that  $\tau_i \propto r_i(r_j - r_k)((\partial_j p)^2 - (\partial_k p)^2)$  which was observed in the results. This leads to  $\frac{\tau_z}{\tau_x} = \frac{r_x - r_y}{r_y - r_z} \frac{r_z}{r_x} \frac{1 - \alpha^2}{\alpha^2} = 1$  from where  $\alpha$  was solved as a function of the aspect ratios. The discrepancy between the two models is explained by the sample finite and by the simplicity of the proposed torque dependency.

#### IV. CONCLUSIONS

The acoustic torque on asymmetric samples in phased array acoustic levitator was determined. The torque calculation method, solving the 3D scattering problem with the boundary element method, allowed one to correctly take into account the finite sample size. A range of simulations over the particle shapes and the field shapes show the range in rotational stiffness of the trap. To achieve the maximum stability, the stiffest trap must be chosen. In addition, a mathematical model was created to predict the results. The model agrees fairly well with the simulation for wide range of aspect ratios. These simulations results allow more reliable orientation control in acoustic levitation.

#### REFERENCES

- [1] E. Brandt, "Acoustic physics: Suspended by sound," *Nature*, vol. 413, no. 6855, p. 474, 2001.
- [2] S. Santesson and S. Nilsson, "Airborne chemistry: Acoustic levitation in chemical analysis," *Analytical and bioanalytical chemistry*, vol. 378, no. 7, pp. 1704–1709, 2004.
- [3] A. Marzo *et al.*, "Holographic acoustic elements for manipulation of levitated objects," *Nature communications*, vol. 6, p. 8661, 2015.
- [4] L. Cox, A. Croxford, B. Drinkwater, and A. Marzo, "Acoustic lock: Position and orientation trapping of non-spherical sub-wavelength particles in mid-air using a single-axis acoustic levitator," *Applied Physics Letters*, vol. 113, no. 5, p. 054 101, 2018.
- [5] G. Maconi *et al.*, "Non-destructive controlled single-particle light scattering measurement," *Journal of Quantitative Spectroscopy and Radiative Transfer*, vol. 204, pp. 159–164, 2018.
- [6] K. Muinonen *et al.*, "Scattering and absorption of light in planetary regoliths," *Journal of Visualized Experiments*, no. 149, p. 59 607, 2019.
- [7] P. Helander *et al.*, "Omnidirectional microscopy by ultrasonic sample control," *unpublished*,
- [8] L. P. Gor'kov, "On the forces acting on a small particle in an acoustical field in an ideal fluid," in *Sov. Phys. Dokl.*, vol. 6, 1962, pp. 773–775.
- [9] H. Bruus, *Theoretical microfluidics*. Oxford university press Oxford, 2008, vol. 18.
- [10] F. B. Wijaya and K.-M. Lim, "Numerical calculation of acoustic radiation force and torque acting on rigid non-spherical particles," *Acta Acustica united with Acustica*, vol. 101, no. 3, pp. 531–542, 2015.